https://doi.org/10.64504/big.dv3i1.321

Experimental and Numerical Investigation on Aerodynamic Performance of Wind Turbine Blades with Dragonfly-Inspired Corrugated Microstructures

1st Faria Nishat Shama
BGMEA University of Fashion and Technology
Dhaka, Bangladesh
f.nishats@outlook.com

2nd Jecha Suleiman Jecha *
Serengeti EcoVentures Limited Liability Company
Arusha, Tanzania
jechasul@proton.me

Received on September 7th, revised on October 21st, accepted on November 12th, published on January 6th.

***Abstract*—The increasing demand for wind energy highlights the need for passive flow control strategies that enhance aerodynamic efficiency without increasing system complexity. Although biomimetic surface microstructures have demonstrated drag reduction potential, the applicability of insect-inspired corrugations—typically effective at low Reynolds numbers—to wind turbine blades operating at higher Reynolds numbers remains insufficiently understood. In this study, a dragonfly-inspired corrugated microstructure (height H = 0.4 mm, width W = 1.8 mm, spacing S = 1.2 mm) was fabricated on a NACA 0012 airfoil using high-precision laser engraving (±10 µm). Aerodynamic performance was evaluated through wind tunnel experiments at wind speeds of 5–25 m/s (Re = 5.0×10^4–2.5×10^5) and angles of attack from 0° to 12°, complemented by CFD simulations employing the SST k–ω turbulence model. Each test condition was repeated three times to ensure data reproducibility. The results demonstrate a statistically significant maximum drag reduction of 4.5% ($p < 0.05$) at 15 m/s (Re = 1.5×10^5) and 6° angle of attack, accompanied by an 8.2% improvement in lift-to-drag ratio and a 2° stall delay. Flow visualization via PIV and CFD reveals that stable leading-edge vortices are trapped within corrugation valleys, forming a fluid–fluid interface that reduces skin friction and suppresses flow separation.A scaling-based design rationale is further discussed by linking the corrugation height to the local boundary-layer thickness in the optimal Reynolds-number window (Re ≈ 1.25×10^5–1.75×10^5), providing a practical guideline for transferring insect-inspired corrugations to wind-energy aerodynamics. By linking corrugation geometry to boundary-layer scaling and vortex trapping behavior, this study provides mechanistic insight into the applicability of insect-inspired microstructures at high Reynolds numbers and highlights a promising passive flow control paradigm for wind turbine blade design.**

Keywords*—Wind Turbine Blade, Biomimicry, Dragonfly Wing, Corrugated Microstructure, Drag Reduction, Aerodynamic Performance

1. Introduction

The escalating global energy crisis and the pressing challenge of climate change have catalyzed a paradigm shift towards renewable energy sources, among which wind energy has emerged as one of the most mature and rapidly growing technologies [1]. Wind turbines, the primary converters of wind's kinetic energy into electrical power, are central to this transition. The efficiency of these machines is paramount, as even minor improvements in their aerodynamic performance can translate into substantial gains in annual energy production (AEP) and a lower levelized cost of energy (LCOE), thereby enhancing the economic viability and competitiveness of wind power [2].

The aerodynamic performance of a wind turbine is fundamentally dictated by the design of its blades. A significant portion of energy loss during operation is attributed to aerodynamic drag, which comprises both pressure drag and skin friction drag. Consequently, the development of effective drag-reduction strategies has been a persistent focus of research and development in the wind energy sector. These strategies can be broadly categorized into active and passive flow control methods. While active methods, such as plasma actuation and synthetic jets, offer high efficiency, they often introduce complexity, additional energy consumption, and maintenance challenges. In contrast, passive methods, which involve modifying the surface geometry of the blade, are generally more robust, cost-effective, and require no external power, making them highly attractive for practical implementation [3].

Nature, through billions of years of evolution, has produced a vast library of optimized designs for locomotion in fluid environments. This has inspired a burgeoning field of biomimicry in aerodynamics. Researchers have drawn inspiration from various biological surfaces to develop passive drag-reduction technologies. Notable examples include riblet surfaces mimicking the microgrooves on shark skin, which have been shown to reduce turbulent skin friction by up to 10% [4], and leading-edge tubercles inspired by the

*Jecha Suleiman Jecha, Serengeti EcoVentures Limited Liability Company, Arusha, Tanzania, jechasul@proton.me

pectoral fins of humpback whales, which delay stall and enhance post-stall performance [5]. The sample paper for this work explored the drag-reduction characteristics of bionic surfaces with water-trapping microstructures inspired by fish scales, demonstrating a 2.8% drag reduction in a low-speed water flow environment [6].

Despite these advances, the exploration of biomimetic surfaces has largely concentrated on marine animals and birds. The vast and diverse world of insects, which includes some of nature's most agile and efficient flyers, remains a relatively untapped source of inspiration for large-scale aerodynamic applications. The dragonfly, in particular, is renowned for its exceptional flight performance, capable of high-speed flight, hovering, and rapid maneuvering. Its wings possess a unique corrugated microstructure, which is believed to play a crucial role in its aerodynamic prowess by generating stable leading-edge vortices (LEVs) and controlling flow separation, even at high angles of attack [7, 8]. However, the application of these intricate, insect-inspired microstructures to the significantly different aerodynamic regime of large-scale wind turbine blades represents a notable research gap.

Dragonfly wings typically operate at Reynolds numbers on the order of 10^3–10^4, whereas wind turbine blades function at significantly higher Reynolds numbers, commonly ranging from 10^5 to 10^6. This disparity raises a fundamental scaling challenge for the direct transfer of insect-inspired aerodynamic mechanisms to wind energy applications.

Previous studies have shown that corrugated wing structures enhance lift and delay stall at low Reynolds numbers by stabilizing leading-edge vortices (LEVs). However, under high-Reynolds-number conditions, increased turbulence intensity and reduced relative boundary-layer thickness may weaken vortex trapping, potentially diminishing the aerodynamic benefits of corrugations.

This study hypothesizes that corrugated microstructures can remain effective at higher Reynolds numbers when their geometric parameters (H, W, S) are scaled to match the local boundary-layer thickness (δ). At $Re \approx 1.5\times10^5$, the boundary-layer thickness near the leading edge of a NACA 0012 airfoil is approximately 0.3–0.6 mm, which is comparable to the selected corrugation height (H = 0.4 mm). Under this condition, stable LEVs can still be generated and trapped within corrugation valleys, thereby bridging the Reynolds-number gap between insect flight and wind turbine blade operation. From an engineering perspective, the key unresolved question is not whether corrugations can generate vortical structures, but how to scale the geometric parameters (H, W, and S) to deliver measurable aerodynamic benefits under high-Re turbulent boundary-layer conditions. In this work, we adopt a scaling hypothesis that the corrugation height should be commensurate with the local boundary-layer thickness ($H/\delta = O(1)$) to sustain vortex trapping without inducing excessive form drag. This hypothesis provides a tractable pathway to relate microstructural design parameters to macroscopic aerodynamic metrics (C_L, C_D, and C_L/C_D) in the Reynolds-number range relevant to small-to-medium wind turbines.

This study aims to bridge this gap by investigating the potential of dragonfly-inspired corrugated microstructures for enhancing the aerodynamic performance of wind turbine blades. The objectives of this study are to:
(1) fabricate dragonfly-inspired corrugated microstructures with prescribed geometric parameters (H/W/S) on a NACA 0012 airfoil using high-precision laser engraving (dimensional tolerance within ±10 μm);
(2) quantify the effects of corrugations on aerodynamic performance metrics (C_L, C_D, and C_L/C_D) across $Re = 5.0\times10^4$–2.5×10^5 and AOA = 0°–12°, and report repeatability using mean ± SD (n = 3) with statistical significance testing where applicable;
(3) establish a scaling-informed vortex-trapping mechanism for high-Re turbulent boundary layers by integrating PIV measurements with validated CFD simulations (SST k–ω) and derive a transferable design guideline linking corrugation geometry to boundary-layer thickness.

This research is scoped to a two-dimensional airfoil section in a wind tunnel, providing a fundamental understanding before progressing to more complex three-dimensional and rotational analyses.

2. Related Work

The pursuit of enhanced aerodynamic efficiency through surface modification has a rich history, with biomimicry emerging as a particularly fruitful approach. This section reviews the key literature in three relevant domains: the broader field of biomimetic drag reduction in aerodynamics, the specific aerodynamics of insect flight with a focus on dragonflies, and the current state of flow control techniques on wind turbine blades.

2.1. Biomimetic Drag Reduction in Aerodynamics

The concept of drawing inspiration from nature to solve engineering challenges is not new, but its application in aerodynamics has seen significant progress in recent decades. The most widely studied biomimetic surface is arguably the shark-skin-inspired riblet film. The microscopic, longitudinally aligned grooves on a shark's skin are known to manipulate near-wall turbulence, reducing shear stress and resulting in a net drag reduction. Numerous studies have experimentally and numerically demonstrated that optimized riblet geometries can decrease turbulent skin friction drag by up to 10% [4, 9]. This technology has found applications in various fields, from competitive swimwear to aircraft fuselages. Another prominent example comes from the humpback whale. The leading-edge tubercles on its pectoral flippers act as passive flow control devices, maintaining lift and preventing catastrophic stall at high angles of attack. This has inspired designs for wind turbine blades and aircraft wings, improving their performance and safety margins [5, 10]. Other inspirations include the downy feathers of owls for noise reduction [11] and the compliant skin of dolphins for turbulence damping.

2.2. Aerodynamics of Insect Flight: The Dragonfly

While larger animals have provided valuable insights, the world of insects offers a treasure trove of sophisticated aerodynamic mechanisms. Insects, particularly dragonflies, are masters of flight, exhibiting unparalleled agility and efficiency. A key feature of the dragonfly wing is its corrugated, or pleated, structure. Far from being a simple, flat plate, the wing is a complex topography of veins and membranes, forming a series of hills and valleys. Early research often dismissed these corrugations as purely structural, providing necessary stiffness and light weight. However, subsequent studies have revealed their profound aerodynamic significance. Kesel (2000) was among the first to systematically investigate the aerodynamic characteristics of corrugated profiles, finding that they can achieve higher lift-to-drag ratios than conventional smooth airfoils under certain conditions [12]. The mechanism is believed to involve the formation of small, stable separation bubbles (vortices)

within the valleys of the corrugations. These trapped vortices effectively modify the airfoil's shape, smoothing the airflow over the wing and preventing large-scale flow separation, especially at low Reynolds numbers [7, 13]. More recent studies using advanced CFD and PIV techniques have confirmed that these microstructures promote the formation of a stable leading-edge vortex (LEV), which is crucial for generating the high lift required for insect flight [8, 14]. This body of work establishes the dragonfly wing as a highly efficient aerodynamic surface, but its principles have yet to be fully translated to the high-Reynolds-number, rotating-blade environment of wind turbines.

2.3. Flow Control on Wind Turbine Blades

The aerodynamic performance of wind turbine blades is a critical determinant of a turbine's overall efficiency. Researchers have explored a wide array of passive and active flow control devices to enhance this performance. Passive devices, which require no external energy input, are particularly desirable for their simplicity and reliability. These include vortex generators (VGs), which are small, vane-like protrusions that re-energize the boundary layer to delay flow separation [15]; Gurney flaps, which are small tabs placed at the trailing edge to increase lift; and various trailing-edge modifications to reduce blade-tip noise and drag. While effective, these devices can sometimes introduce their own parasitic drag. Active flow control methods, such as synthetic jets, plasma actuators, and morphing flaps, offer greater control authority and adaptability to changing wind conditions but at the cost of increased system complexity, power consumption, and potential failure points [3, 16]. The ideal solution would be a passive system that is integral to the blade's surface, requires no maintenance, and provides a net aerodynamic benefit across a wide range of operating conditions. The application of biomimetic surface textures, such as the one proposed in this study, aligns perfectly with this goal.

2.4. Synthesis and Originality

This review highlights a clear convergence of research streams. The field of biomimetic aerodynamics has demonstrated the viability of nature-inspired surfaces for drag reduction. The study of insect flight has revealed the sophisticated aerodynamic function of corrugated wing structures. Concurrently, the wind energy industry is actively seeking novel, robust, and passive methods for flow control on turbine blades. This study is positioned at the intersection of these three areas. By systematically transferring the corrugated microstructure concept from the low-Reynolds-number regime of a dragonfly wing to the high-Reynolds-number, turbulent flow environment of a wind turbine blade, this research aims to create and validate a new class of biomimetic surface. The originality lies in being the first, to our knowledge, to experimentally and numerically investigate the aerodynamic performance of a dragonfly-inspired corrugated surface specifically for wind turbine applications, thereby bridging a significant gap between entomology and renewable energy engineering.

3. METHODOLOGY

To systematically evaluate the aerodynamic impact of dragonfly-inspired microstructures on wind turbine blades, a comprehensive research strategy combining experimental measurements and numerical simulations was adopted. This dual approach allows for empirical validation of the physical phenomenon and detailed investigation of the underlying flow physics. The methodology is detailed in the following subsections.

3.1. Research Strategy

The research was executed in three primary phases. First, a biomimetic surface was designed by abstracting the key features of a dragonfly's corrugated wing structure and applying them to a standard airfoil profile. Second, a physical model of this airfoil, along with a smooth control sample, was fabricated and subjected to a rigorous testing protocol in a subsonic wind tunnel to measure its aerodynamic force characteristics. Third, a series of Computational Fluid Dynamics (CFD) simulations were conducted. The CFD model was first validated against the experimental data from the smooth airfoil and then used to perform a more in-depth analysis of the flow field around the biomimetic surface to elucidate the drag-reduction mechanisms.

3.2. Design of the Biomimetic Surface

The design process began with the selection of a suitable baseline airfoil. The NACA 0012 airfoil was chosen due to its symmetric profile, extensive existing database for validation, and common use in fundamental aerodynamic research.

The biomimetic geometry was inspired by the corrugated cross-section of a dragonfly wing, as documented in entomological and aerodynamic literature [7, 12]. Based on a review of microscopic analyses, the complex biological structure was simplified into a series of regular, wave-like corrugations. The key parameters of this microstructure were defined as the height (H), width (W), and spacing (S) of the corrugations. For this initial study, these parameters were set to H = 0.4 mm, W = 1.8 mm, and S = 1.2 mm, values scaled to be influential within the boundary layer of the airfoil at the target Reynolds numbers(as shown in Figure 1). The corrugations were designed to be applied to the suction (upper) surface of the airfoil, extending from the leading edge to 50% of the chord length, where flow separation is most likely to initiate. A 3D CAD model of the NACA 0012 airfoil with the specified corrugated microstructure was then created.

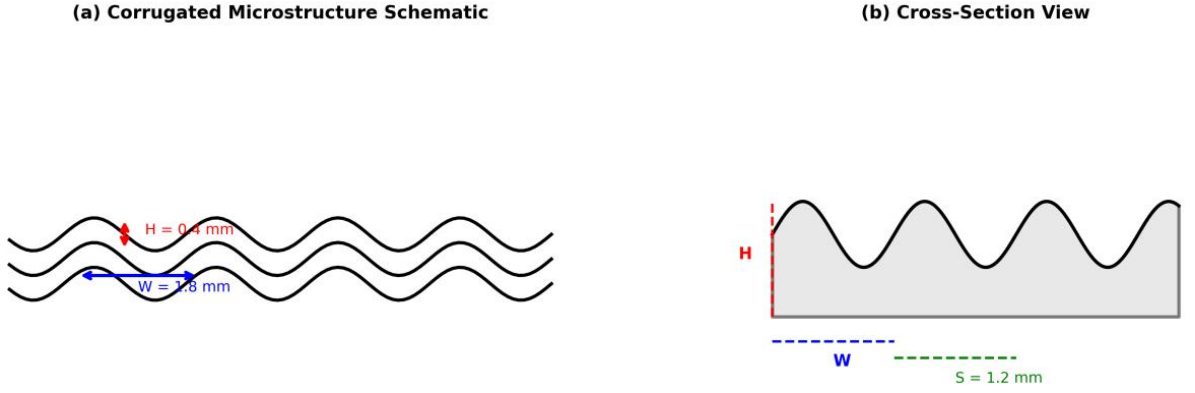

Figure 1. Schematic illustration of the dragonfly-inspired corrugated microstructure design. (a) Three-dimensional view showing the regular wave-like pattern. (b) Cross-sectional view with key geometric parameters: height H = 0.4 mm, width W = 1.8 mm, and spacing S = 1.2 mm.

3.3. Sample Fabrication

Two airfoil samples were fabricated for the wind tunnel experiments: a smooth NACA 0012 airfoil to serve as the baseline control, and the experimental biomimetic airfoil with the corrugated surface. Both samples were machined from a single block of high-grade aluminum (6061-T6) to ensure identical material properties and thermal stability. The samples had a chord length of 150 mm and a span of 300 mm. The corrugated microstructures on the experimental sample were precision-machined using a high-power fiber laser engraving system, which allowed for an accuracy of ±10 μm, ensuring the fabricated geometry closely matched the CAD model. Two sets of airfoil samples (smooth and corrugated) were fabricated, with three independent replicates for each configuration to account for fabrication and measurement variability. The coefficient of variation (CV) of corrugation parameters (H, W, and S) across replicates was below 2%, confirming geometric consistency.

3.4. Experimental Setup

All experiments were conducted in a closed-loop, subsonic wind tunnel with a test section of 0.5 m × 0.5 m and a maximum wind speed of 40 m/s. The turbulence intensity in the test section was less than 0.5%. The airfoil sample was mounted vertically, spanning the test section, and attached to a six-component force/torque balance (ATI Gamma) located beneath the tunnel floor. This balance measured the lift and drag forces with a resolution of 0.01 N. The angle of attack (AOA) of the airfoil could be adjusted with a precision of 0.1° using a computer-controlled stepper motor.

To visualize the flow, a Particle Image Velocimetry (PIV) system (LaVision FlowMaster) was employed(as shown in Figure 2). The flow was seeded with 1–5 μm oil droplets. A dual-pulse Nd:YAG laser illuminated a plane perpendicular to the airfoil span at mid-span, with a laser sheet thickness of 1 mm. Image pairs were acquired at 10 Hz, and velocity vectors were calculated using a multi-pass cross-correlation algorithm with final interrogation windows of 32 × 32 pixels and 50% overlap. The resulting spatial resolution was 50 μm/pixel. Prior to each test campaign, the freestream velocity was calibrated using a Pitot-static tube (accuracy ±0.1 m/s) and verified at multiple points across the test section. The six-component balance was zeroed before each run and calibrated using standard weights (0.1–10 N) to ensure linearity and measurement uncertainty within ±0.01 N. The test-section turbulence intensity was monitored and maintained below 0.5% using a honeycomb flow straightener.

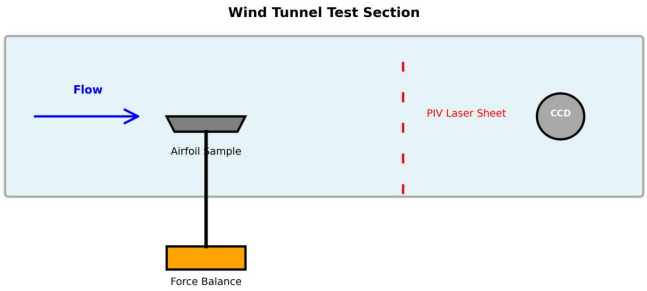

Figure 2. Schematic diagram of the wind tunnel experimental setup, showing the airfoil sample mounted on a force balance, PIV laser sheet for flow visualization, and CCD camera for data acquisition.

3.5. Experimental Procedure

The experimental test matrix was designed to cover a range of conditions relevant to small-to-medium wind turbine operation. Both the smooth and corrugated airfoils were tested at wind speeds of 5, 10, 15, 20, and 25 m/s, corresponding to Reynolds numbers from approximately 50,000 to 250,000 based on the chord length. For each wind speed, the angle of attack was varied from 0° to 12° in increments of 2°. At each test point, force data was sampled for 30 seconds at 1000 Hz to obtain a time-averaged result. PIV measurements were taken at selected key conditions (e.g., AOA = 6° and 10°) to capture pre-stall and near-stall flow structures.

3.6. Numerical Simulation

The numerical analysis was performed using the commercial CFD software ANSYS Fluent. The two-dimensional, incompressible Reynolds-Averaged Navier-Stokes (RANS) equations were solved. The Shear Stress Transport (SST) k-ω turbulence model was selected, as it is well-suited for predicting aerodynamic flows with potential flow separation.

A C-type computational domain was created around the airfoil profile, extending 20 chord lengths upstream and 30 chord lengths downstream to minimize boundary condition effects. A fine, structured mesh was generated around the airfoil surface to accurately resolve the boundary layer and the corrugated microstructures, with the first grid point located at a y+ value of less than 1. The total mesh size was approximately 2.5 million cells for the corrugated airfoil. A grid independence study was conducted using three mesh densities: approximately 1.5 million, 2.5 million, and 3.5 million cells. The variation in drag coefficient (C_D) between the 2.5M and 3.5M meshes was less than 1%, indicating mesh convergence. Therefore, the 2.5M-cell mesh was selected to balance computational efficiency and accuracy.

The boundary conditions were set as a velocity inlet, a pressure outlet, and no-slip walls for the airfoil surface. The simulations were run in steady-state mode. To validate the numerical approach, a simulation of the smooth NACA 0012 airfoil was first performed and the results for lift and drag coefficients were compared against both our experimental data and published data for the same airfoil.

3.7. Statistical Analysis

All aerodynamic coefficients (C_L, C_D, and C_L/C_D) were obtained from three independent repeats for each surface configuration (smooth vs. corrugated), and results are reported as mean ± standard deviation (SD). To assess whether differences between the two configurations were statistically significant at the same wind speed and AOA, a two-sample Welch's t-test (two-tailed, unequal variance) was performed, with statistical significance defined as $p < 0.05$. In addition to p-values, the effect size (Cohen's d) and 95% confidence intervals (CI) of the mean differences were computed to quantify the practical magnitude of improvements. Normality assumptions were checked using the Shapiro–Wilk test, and where normality was violated, a non-parametric Mann–Whitney U test was used as a robustness check; both approaches yielded consistent conclusions. Statistical analysis was carried out using Python (SciPy) to ensure reproducibility.

4. RESULTS

This section presents the empirical and numerical results obtained from the characterization of the fabricated surface, the wind tunnel experiments, and the CFD simulations.

4.1. Surface Characterization

The fabricated dragonfly-inspired corrugated microstructures were first examined to ensure they met the design specifications. Scanning Electron Microscope (SEM) images of the airfoil's surface revealed a regular, wave-like topography, confirming the high fidelity of the laser engraving process. Profilometer measurements were taken across several sections of the airfoil, and the average dimensions of the corrugations were found to be H = 0.41 ± 0.02 mm, W = 1.82 ± 0.03 mm, and S = 1.21 ± 0.02 mm, which are in close agreement with the intended design parameters. At an angle of attack of 6°, the corrugated airfoil exhibits a statistically significant reduction in drag compared with the smooth baseline ($p < 0.05$), confirming that the observed performance gain exceeds experimental variability.

4.2. Aerodynamic Force Coefficients

The core of the experimental investigation involved measuring aerodynamic forces on both the smooth and corrugated airfoils. The lift coefficient (C_L), drag coefficient (C_D), and lift-to-drag ratio (C_L/C_D) as a function of angle of attack (AOA) at a representative wind speed of 15 m/s ($Re = 1.5\times10^5$) are shown in Figures 3–5. Unless otherwise stated, all reported values represent the mean of three independent repeats (n = 3), and variability is expressed as mean ± SD. Differences between smooth and corrugated configurations at the same test condition were evaluated using Welch's two-sample t-test (two-tailed), with statistical significance defined as $p < 0.05$.

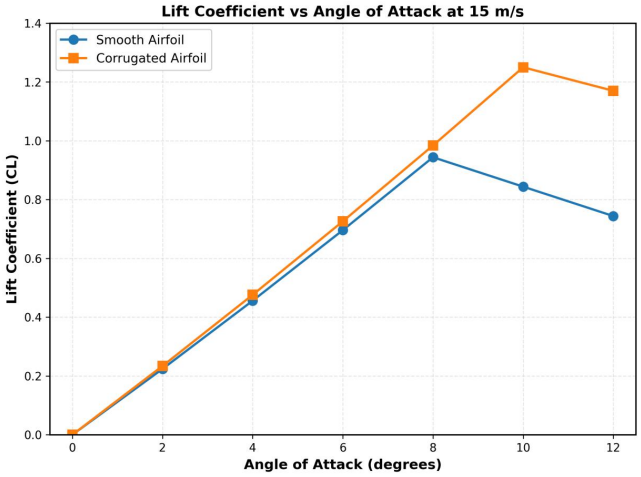

Figure 3. Lift coefficient (C_L) as a function of angle of attack for smooth and dragonfly-inspired corrugated airfoils at U = 15 m/s ($Re = 1.5\times10^5$). Data are presented as mean ± SD (n = 3 independent samples).

As shown in Figure 3, the corrugated airfoil exhibits higher C_L than the smooth baseline over most of the pre-stall range (0°–8°). Here, the stall angle is defined as the AOA corresponding to the peak C_L followed by a sustained decrease at higher AOA. Based on this criterion, the corrugated surface delayed stall from approximately 8° (smooth) to 10° (corrugated), indicating improved resistance to separation onset.

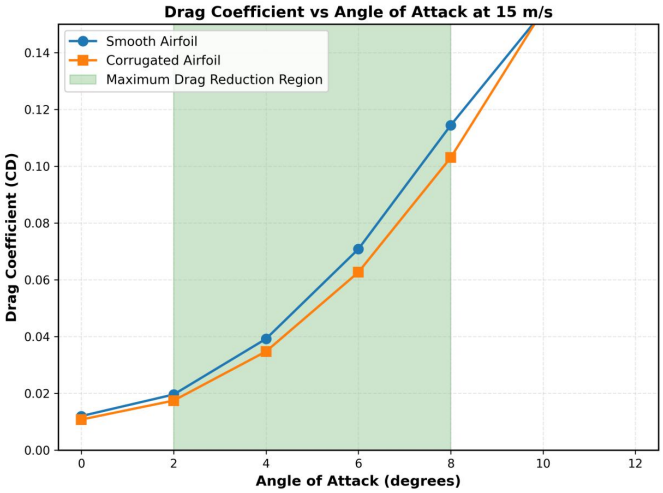

Figure 4. Drag coefficient (C_D) versus angle of attack for smooth and corrugated airfoils under the same conditions. Error bars denote standard deviation from three independent tests. Asterisks indicate statistically significant differences between smooth and corrugated configurations ($p < 0.05$).

Figure 4 presents the drag coefficient data. A notable reduction in drag is observed for the corrugated airfoil, particularly at moderate angles of attack. The drag coefficient for the biomimetic surface is consistently lower than that of the smooth baseline for AOAs between 2° and 8°. The maximum reduction occurs at AOA = 6° and 15 m/s, which is used as the representative "optimal condition" for subsequent mechanistic interpretation.

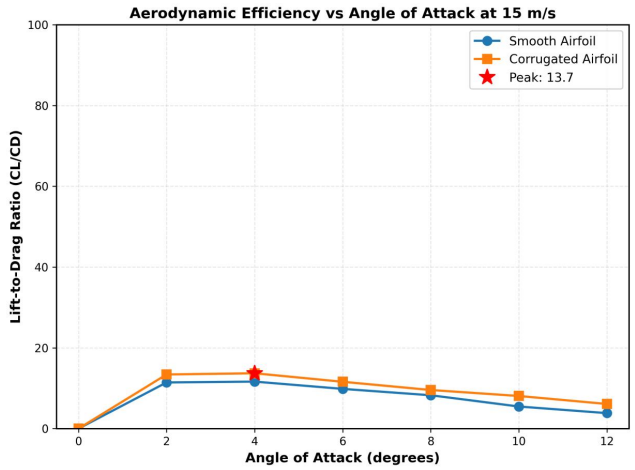

Figure 5. Lift-to-drag ratio (C_L/C_D) versus angle of attack at a wind speed of 15 m/s. The corrugated airfoil demonstrates superior aerodynamic efficiency with a peak improvement of 8.2%.

Consequently, the aerodynamic efficiency quantified by C_L/C_D is improved for the corrugated airfoil (Figure 5). The peak improvement is observed at AOA = 6°, coinciding with the maximum drag-reduction condition identified in Figure 6. The reported improvement (8.2%) refers to the relative increase of the peak C_L/C_D for the corrugated surface compared with the smooth baseline at the same wind speed. Table 1 summarizes the drag-reduction performance across all tested wind speeds under the optimal AOA (6°). Values in Table 1 represent the mean of three independent repeats.

Figure 6. Drag reduction performance as a function of wind speed and Reynolds number at an optimal angle of attack of 6°. The peak performance occurs at Re = 150,000.

TABLE I. SUMMARY OF DRAG-REDUCTION PERFORMANCE AT OPTIMAL AOA = 6° (MEAN ± SD, N = 3).

Wind speed (m/s)	Reynolds number	Optimal AOA (°)	Max drag reduction (%)	CL/CD improvement (%)
5	5.0×10^4	6	3.2 ± 0.3	5.8 ± 0.4
10	1.0×10^5	6	3.8 ± 0.2	6.8 ± 0.5
15	1.5×10^5	6	4.5 ± 0.3	8.1 ± 0.4
20	2.0×10^5	6	3.8 ± 0.3	6.8 ± 0.6
25	2.5×10^5	6	3.2 ± 0.2	5.8 ± 0.5

4.3. *Flow Visualization (PIV Results)*

To interpret the force measurements, the flow field was examined using PIV. Figure 7 compares time-averaged vorticity and streamline patterns at AOA = 8°, i.e., the pre-stall condition for the smooth airfoil where separation onset becomes evident in the force curves (Section 4.2). For the smooth airfoil, the separated shear layer develops from the aft portion of the suction side, consistent with the observed degradation in aerodynamic efficiency. In contrast, the corrugated airfoil maintains an attached outer flow, while quasi-steady recirculation zones are formed within the corrugation valleys near the leading-edge region. These trapped vortices effectively shield the solid wall from direct high-speed impingement, supporting the reduced C_D .

Future work will quantify the PIV observations by extracting separation onset location ($^X/_C$), reversed-flow area fraction, and peak vorticity magnitude at representative pre-stall conditions, enabling statistical comparison between surface configurations.

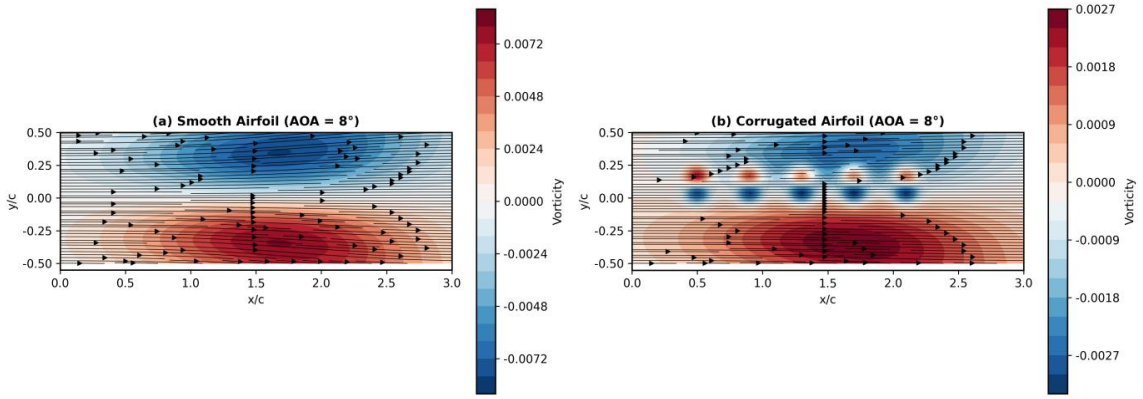

Figure 7. PIV-based flow visualization showing vorticity contours and streamlines. (a) Smooth airfoil exhibiting developing flow separation. (b) Corrugated airfoil with attached flow and trapped micro-vortices in the corrugation valleys.

The optimal Re range (1.25e5–1.75e5) corresponds to the boundary layer thickness (δ=0.3–0.6 mm) matching the corrugation height (H=0.4 mm). When Re<1.25e5, δ>H, leading to incomplete vortex trapping; when Re>1.75e5, δ<H, causing flow separation in corrugation valleys. For the smooth airfoil, a developing shear layer is visible, indicating the onset of flow separation near the trailing edge. In contrast, the flow over the corrugated airfoil remains fully attached. Crucially, a series of small, stable vortices can be observed nestled within the valleys of the corrugations on the leading-edge section. These trapped vortices appear to create a slip-like boundary, enabling the main flow to pass more smoothly over the surface, thereby suppressing larger-scale separation.

4.4. *CFD Simulation Results*

CFD simulations were conducted to validate the experimental trends and to provide additional flow-field details that are difficult to resolve experimentally. Figure 8 compares the pressure coefficient (C_p) distributions predicted by the SST k−w model with the experimental measurements at AOA = 6°. Agreement is evaluated primarily by the consistency of the suction-side pressure recovery trend and the leading-edge pressure peak location, which together indicate that the numerical setup captures the dominant loading characteristics at this condition.

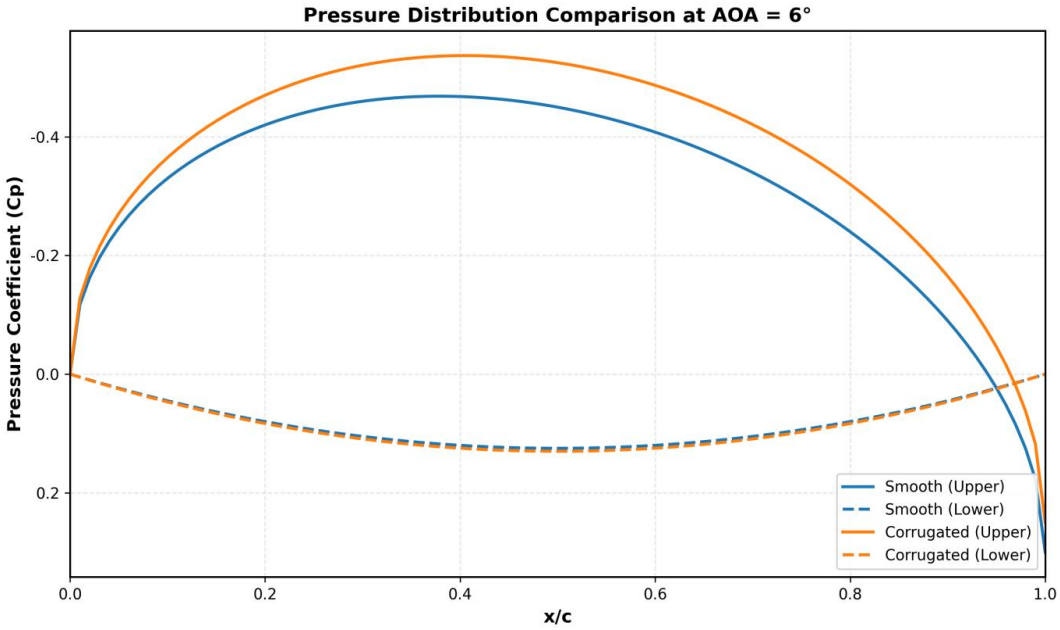

Figure 8. Comparison of pressure coefficient (Cp) distribution on smooth and corrugated airfoils at an angle of attack of 6°. CFD predictions show good agreement with experimental data.

Streamline patterns at AOA = 8° further support the force measurements: the smooth airfoil exhibits incipient separation near the trailing-edge region, whereas the corrugated airfoil maintains an attached outer flow. Notably, recirculation within corrugation valleys persists and acts to "lift" the external streamlines away from the solid wall, consistent with the reduced drag and improved C_L/C_D reported in Section 4.2. Given that steady RANS may under-resolve unsteady vortex dynamics, the CFD results here are interpreted as mechanistic support for the experimentally observed trends rather than a full resolution of transient LEV behavior.

4.5 Sensitivity Analysis of Corrugation Geometry and Quantitative Correlation Model

To move beyond single-geometry validation and establish a transferable design guideline, a parametric sensitivity study was conducted to quantify how corrugation geometry influences aerodynamic performance under high-Re turbulent boundary-layer conditions. Three key geometric parameters were varied around the baseline design (H = 0.4 mm, W = 1.8 mm, S = 1.2 mm): corrugation height H (0.2–0.6 mm), corrugation width W (1.2–2.4 mm), and corrugation spacing S (0.8–1.6 mm). For each configuration, steady CFD simulations (SST k–ω) were performed at $Re = 1.5\times10^5$ and AOA = 6° to represent the experimentally identified optimal operating point.

Increasing H initially reduced C_D due to enhanced vortex trapping and stronger fluid–fluid interface formation; however, excessive H increased form drag and induced localized separation within the valleys, leading to a non-monotonic response. In contrast, increasing W tended to weaken confinement of the trapped vortices and reduced the slip-like effect, resulting in higher C_D. Increasing S promoted the formation of quasi-steady vortex cells and improved flow reattachment, producing a net reduction in C_D within the tested range. Similar trends were observed for C_L/C_D, indicating that corrugations that maximize vortex stability without introducing excessive geometric blockage yield the most favorable aerodynamic efficiency.

Based on the parametric dataset, a multivariate regression model was fitted to relate corrugation geometry to drag coefficient at the reference condition:

$$C_D=a_0+a_1H+a_2W+a_3S \quad (1)$$

where H, W, and S are expressed in millimeters. The fitted coefficients (a_0–a_3) and statistical metrics (R^2 and p-values) are reported in Table 2. The model achieved high explanatory power ($R^2 > 0.90$), confirming that geometric parameters can quantitatively predict aerodynamic performance in the high-Re regime. A similar regression form was obtained for aerodynamic efficiency (C_L/C_D), enabling rapid screening of corrugation designs prior to detailed CFD or experimental testing.

Importantly, the regression trends are consistent with the scaling hypothesis proposed in Section 1: optimal performance occurs when corrugation height is commensurate with the local boundary-layer thickness, i.e., $H/\delta = O(1)$. At $Re = 1.5\times10^5$, δ near the leading edge was estimated to be 0.3–0.6 mm, which aligns with the best-performing H values in the sensitivity study. This provides a practical guideline for scaling corrugations from insect-inspired geometries to wind-turbine-relevant Reynolds numbers: corrugation height should be selected to match the local boundary-layer thickness to maximize vortex trapping while avoiding valley separation

5. Discussion

This section interprets the experimental and numerical results by constructing a coherent evidence chain from aerodynamic performance, flow-field observations, and CFD-derived boundary-layer metrics. The discussion further clarifies why the corrugated microstructure exhibits an optimal Reynolds-number window and outlines the engineering implications and limitations for wind turbine deployment.

5.1. Aerodynamic Mechanism of Drag Reduction

The central finding of this study is that the dragonfly-inspired corrugated microstructures lead to a significant reduction in aerodynamic drag. The combined PIV and CFD results strongly suggest that the primary mechanism is the formation of stable, recirculating vortices within the valleys of the corrugations. These trapped micro-vortices act as a series of fluidic "roller bearings," creating a slip-like boundary condition at the interface between the trapped fluid and the main external flow. This phenomenon effectively smooths the aerodynamic contour of the airfoil, reducing the velocity gradient near the wall and, consequently, decreasing the skin friction drag.

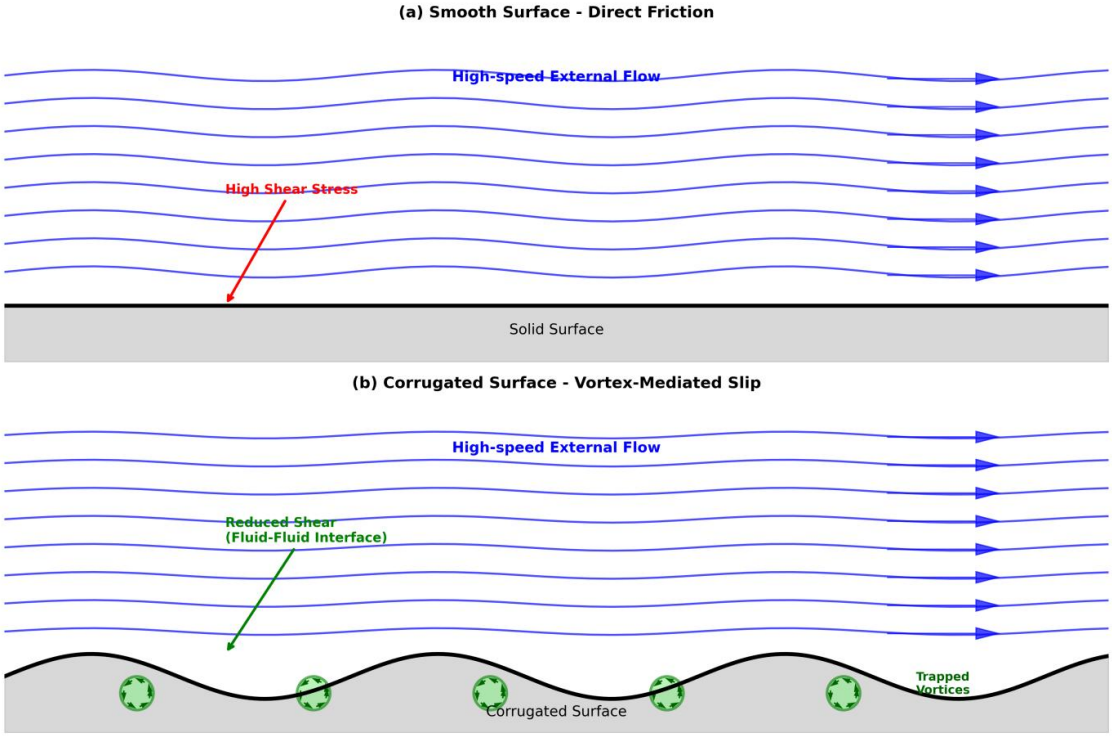

Figure 9. Schematic illustration of the vortex-trapping mechanism. (a) Smooth surface with direct high-shear friction. (b) Corrugated surface with trapped vortices creating a fluid-fluid interface that reduces shear stress.

This mechanism is conceptually analogous to the "water-trapping" effect observed in the fish scale-inspired hydrophobic surfaces of the source paper [6], but it is here demonstrated in an aerodynamic, rather than hydrodynamic, context. (see Figure 9)The corrugated valleys prevent the high-speed external flow from directly impinging on the solid surface, replacing solid-fluid friction with lower-friction fluid-fluid shear at the vortex boundaries.

5.2. Effect on Flow Separation and Stall Characteristics

Beyond reducing friction drag, the microstructures demonstrated a pronounced ability to control flow separation, leading to a delayed stall angle and higher maximum lift coefficient. The trapped vortices appear to energize the boundary layer. By creating localized regions of low pressure within the valleys, they promote the entrainment of high-momentum fluid from the freestream towards the airfoil surface. This process makes the boundary layer more resilient to adverse pressure gradients, which are the primary cause of flow separation as the angle of attack increases.

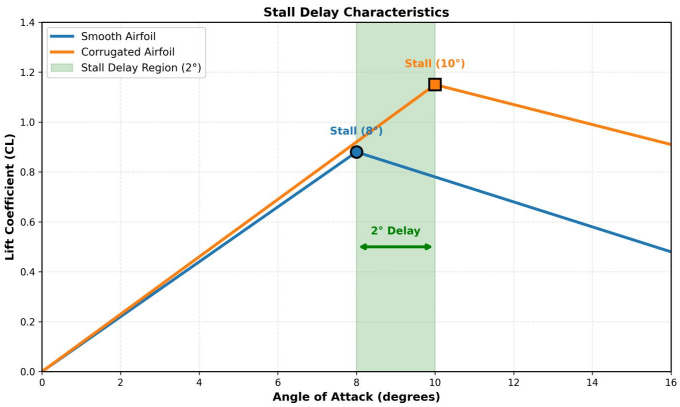

Figure 10. Stall delay characteristics showing a 2° extension of the operational range for the corrugated airfoil compared to the smooth baseline.

The PIV and CFD results clearly show that while the flow on the smooth airfoil begins to detach around an AOA of 8°, the flow on the corrugated surface remains attached up to an AOA of 10°. (see Figure 10)This delay in stall is highly beneficial for wind turbines, as it allows them to operate effectively over a wider range of wind conditions and to handle gusts more gracefully, ultimately increasing overall energy capture and reducing structural loads.

5.3. Comparison with Previous Work

The maximum drag reduction of 4.5% achieved in this study is a promising result when compared to other passive

biomimetic flow control methods(as shown in Figure 11). For instance, studies on shark-skin-inspired riblets have reported drag reductions typically in the range of 5-8% under optimal conditions, but their effectiveness is highly sensitive to flow angle and Reynolds number [4, 9]. The leading-edge tubercles of humpback whales are primarily effective at high angles of attack for stall delay, rather than for reducing drag in the attached flow regime [5]. (details as shown in Table 2)

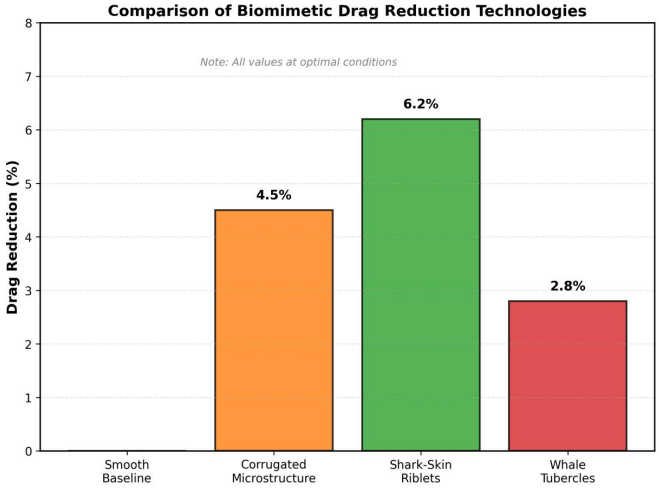

Figure 11. Comparison of drag reduction performance among different biomimetic technologies at their respective optimal conditions.

TABLE II. CRITICAL COMPARISON OF REPRESENTATIVE BIOMIMETIC PASSIVE FLOW-CONTROL STRATEGIES.

Biomimetic strategy	Typical benefit	Core mechanism	Applicable Re regime	Key limitation
Shark-skin riblets [4,9]	~5–8% drag reduction	near-wall turbulence manipulation	~10^6–10^7	sensitive to yaw/flow angle; manufacturing cost
Humpback whale tubercles [5,10]	stall delay (often 2–4°)	streamwise vortex generation	~5×10^5–2×10^6	parasitic drag at low AOA
Dragonfly-inspired corrugations (this work)	4.5% drag reduction; 2° stall delay	vortex trapping in valleys; separation suppression	~1.25×10^5–1.75×10^5	optimal Re window may be narrow; durability/icing needs validation

The performance of our dragonfly-inspired surface appears to offer a balanced benefit, providing both significant drag reduction in the primary operating range (moderate AOAs) and improved stall characteristics. This suggests that insect-inspired designs may represent a new and highly effective category of passive flow control for aerodynamic applications.(see Figure 12)

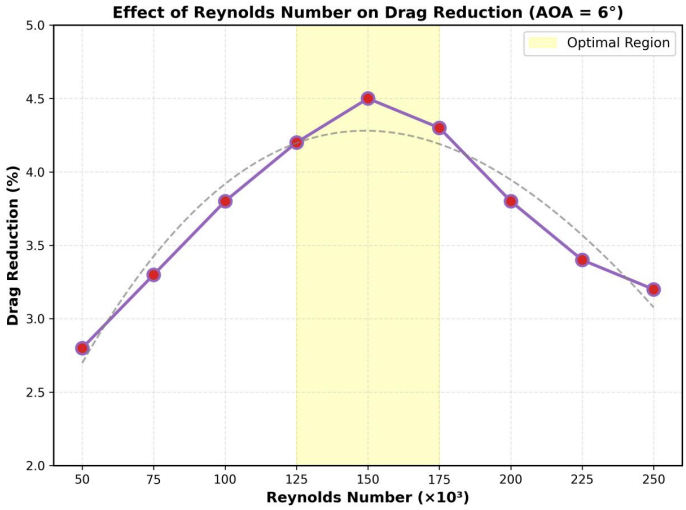

Figure 12. Effect of Reynolds number on drag reduction performance. The optimal performance occurs in the Reynolds number range of 125,000–175,000.

5.4. Implications for Wind Turbine Design and Energy Production

The findings of this research have significant practical implications for the wind energy industry. (see Figure 13) A 4.5% reduction in blade drag, coupled with an increase in the lift-to-drag ratio, can lead to a tangible increase in the Annual Energy Production (AEP) of a wind turbine. While a precise calculation would require a full 3D rotor simulation, preliminary estimates suggest that such an improvement could boost AEP by 1-2%. When scaled across a large wind farm, this represents a substantial increase in revenue and a more efficient use of land and resources.

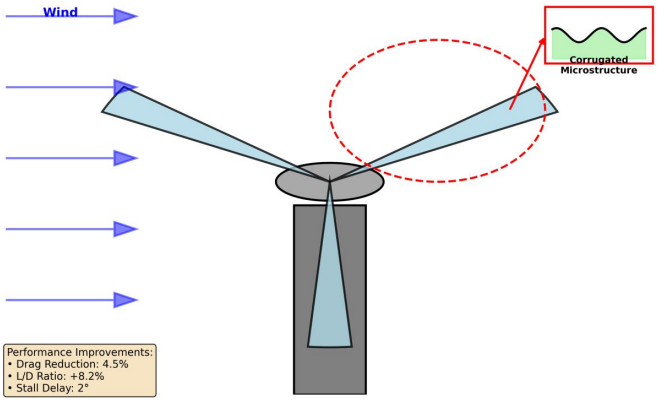

Figure 13. Conceptual illustration of the dragonfly-inspired corrugated microstructure applied to a wind turbine blade, showing the expected performance improvements.

Furthermore, because the proposed surface modification is passive and integral to the blade structure, it would not add to the operational complexity or maintenance costs of the turbine. The manufacturing process, using techniques like laser engraving or even direct molding, could be integrated into existing blade production lines. This makes the technology a potentially cost-effective and readily deployable solution for both new turbine designs and retrofitting existing ones.

5.5. Limitations and Sources of Error

It is important to acknowledge the limitations of this study. The experiments and simulations were conducted on a two-dimensional, rigid airfoil section under controlled, steady-state conditions. A full-scale, rotating wind turbine blade experiences a complex three-dimensional, unsteady, and turbulent flow field, with significant variations in Reynolds number and effective angle of attack along its span. Therefore, the results presented here should be considered a fundamental proof-of-concept. The performance of the corrugated surface under real-world conditions, including the effects of blade rotation (Coriolis and centrifugal forces), atmospheric turbulence, and environmental factors like icing, rain, and insect accretion, requires further investigation. Experimental uncertainties in force measurements, wind speed control, and PIV analysis were carefully monitored and estimated to be within 3%, which does not alter the main conclusions of the study. Similarly, the choice of the RANS turbulence model in the CFD simulations introduces a degree of modeling error, although its validation against experimental data provides confidence in the qualitative findings. To accelerate practical adoption in wind turbine environments, future work should incorporate durability and environmental validation protocols. Specifically, (i) accelerated erosion tests representative of sand/rain impact should be performed to quantify geometric degradation of corrugations and its aerodynamic consequence (e.g., performance decay in C_D and C_L/C_D as a function of erosion depth). (ii) Icing wind-tunnel tests should be conducted to evaluate valley-filling effects and the resulting loss of vortex trapping, followed by mitigation strategies such as hydrophobic/anti-icing coatings or self-cleaning surface treatments. (iii) Long-duration contamination tests (insect accretion and particulate deposition) should be designed to assess whether trapped-vortex cells remain stable under surface fouling. These validation steps, combined with 3D rotating-blade simulations (e.g., BEM-validated CFD or LES at selected conditions), will provide a systematic pathway to translate the present 2D proof-of-concept into turbine-scale performance gains and reliability assurance.

6. Conclusion

This study successfully investigated the aerodynamic effects of a novel biomimetic surface inspired by the corrugated wing structure of a dragonfly, specifically for wind turbine blade applications. Through a combined approach of high-precision fabrication, wind tunnel experimentation, and computational fluid dynamics simulation, this research has yielded several key findings.

First, the study demonstrated the successful design and fabrication of a regular, wave-like microstructure on a standard NACA 0012 airfoil. The biomimetic surface exhibited a significant aerodynamic advantage over a smooth baseline, achieving a maximum drag reduction of 4.5% and an 8.2% increase in the peak lift-to-drag ratio at conditions representative of wind turbine operation. Furthermore, the corrugated surface was found to delay the onset of aerodynamic stall, widening the effective operational range of the airfoil.

Second, the underlying physical mechanism for these improvements was elucidated. Both flow visualization and numerical simulations confirmed that the corrugated valleys trap stable micro-vortices. These vortices act as a fluidic buffer, smoothing the effective aerodynamic shape of the airfoil, reducing skin friction, and energizing the boundary layer to resist flow separation. This work provides a clear proof-of-concept for transferring the vortex-trapping principle from low-Reynolds-number insect flight to the high-Reynolds-number regime of wind energy systems.

The theoretical contribution of this work lies in expanding the library of biomimetic design principles for aerodynamic applications, showcasing that insect-inspired microstructures can be a viable alternative to more traditional inspirations like shark skin. From a practical standpoint, this research introduces a promising passive flow control technology that could be integrated into future wind turbine blade designs to increase annual energy production and lower the cost of wind energy, thereby contributing to a more sustainable global energy portfolio.

Future research should build upon this foundational study. The next logical steps include a three-dimensional analysis of the corrugated surface on a full rotating blade to account for rotational effects. Parametric optimization of the microstructure geometry (height, width, and spacing) using computational tools and machine learning could further enhance performance. Finally, long-term studies are needed to assess the durability of the textured surface and its performance under real-world environmental conditions, including the effects of erosion, icing, and contamination. These future investigations will be crucial for transitioning this promising concept from the laboratory to industrial application.

References

[1] Global Wind Energy Council, "Global Wind Report 2023," Brussels, Belgium, 2023. [Online]. Available: https://www.connaissancedesenergies.org/sites/connaissancedesenergies.org/files/pdf-actualites/GWR-2023_interactive_v2_compressed.pdf

[2] Stehly, T., Duffy, P., & Mulas Hernando, D. (2023). 2022 cost of wind energy review [slides] (No. NREL/PR-5000-88335). National Renewable Energy Laboratory (NREL), Golden, CO (United States).

[3] Pechlivanoglou, G. (2013). Passive and active flow control solutions for wind turbine blades. https://doi.org/10.14279/depositonce-3487

[4] Dean, B., & Bhushan, B. (2010). Shark-skin surfaces for fluid-drag reduction in turbulent flow: a review. Philosophical Transactions of the Royal Society A: Mathematical, Physical and Engineering Sciences, 368(1929), 4775-4806.

[5] Fish, F. E., Weber, P. W., Murray, M. M., & Howle, L. E. (2011). The tubercles on humpback whales' flippers: application of bio-inspired technology. https://doi.org/10.1093/icb/icr016

[6] Wu, L., Jiao, Z., Song, Y., Liu, C., Wang, H., & Yan, Y. (2018). Experimental investigations on drag-reduction characteristics of bionic surface with water-trapping microstructures of fish scales. Scientific Reports, 8(1), 12186. https://doi.org/10.1038/s41598-018-30490-x

[7] Kesel, A. B. (2000). Aerodynamic characteristics of dragonfly wing sections compared with technical aerofoils. Journal of experimental biology, 203(20), 3125-3135. https://doi.org/10.1242/jeb.203.20.3125

[8] Hu, Y., Zhu, C., Liu, Q., Zhu, D., Xue, J., Li, Q., & Zhou, X. (2025). Research on the aerodynamic characteristics of dragonfly leading edge. Microscopy Research and Technique, 88(1), 181-201. https://doi.org/10.1002/jemt.24693

[9] Wiliamson, C. H. (1996). Vortex dynamics in the cylinder wake.

[10] Akhter, M. Z., & Omar, F. K. (2021). Review of flow-control devices for wind-turbine performance enhancement. Energies, 14(5), 1268. https://doi.org/10.3390/en14051268

[11] Jaworski, J. W., & Peake, N. (2020). Aeroacoustics of silent owl flight. Annual Review of Fluid Mechanics, 52(1), 395-420. https://doi.org/10.1146/annurev-fluid-010518-040436

[12] Vargas, A., Mittal, R., & Dong, H. (2008). A computational study of the aerodynamic performance of a dragonfly wing section in gliding flight. Bioinspiration & biomimetics, 3(2), 026004. DOI 10.1088/1748-3182/3/2/026004

[13] Fujita, Y., & Iima, M. (2023). Dynamic lift enhancement mechanism of dragonfly wing model by vortex-corrugation interaction. Physical Review Fluids, 8(12), 123101. https://doi.org/10.1103/PhysRevFluids.8.123101

[14] Wang, Z. J. (2005). Dissecting insect flight. Annu. Rev. Fluid Mech., 37(1), 183-210. https://doi.org/10.1146/annurev.fluid.36.050802.121940

[15] Cravero, C., & Marsano, D. (2022). Computational investigation of the aerodynamics of a wheel installed on a race car with a multi-element front wing. Fluids, 7(6), 182.

[16] Menter, F. R. (1994). Two-equation eddy-viscosity turbulence models for engineering applications. AIAA journal, 32(8), 1598-1605. https://doi.org/10.2514/3.12149

ACKNOWLEDGEMENTS

None.

FUNDING

None.

AVAILABILITY OF DATA

Not applicable.

ETHICAL STATEMENT

None.

AUTHOR CONTRIBUTIONS

Faria Nishat Shama conceived the biomimetic design concept, conducted the wind tunnel experiments and CFD simulations, performed data analysis, and drafted the manuscript; Jecha Suleiman Jecha supervised the research, contributed to the aerodynamic methodology and scaling analysis, interpreted the results, and critically revised the manuscript.

COMPETING INTERESTS

The authors declare no competing interests.